PAPER

Check for updates

Hydroxypropyl-β-cyclodextrin-incorporated Pebax composite membrane for improved permselectivity in organic solvent nanofiltration†

Mengmeng Jia,[a] Yucang Liang, [ID] *[b] Ziyang Liu,[a] Yue Liu, [ID] [a] Xuehong Zhang[a] and Hongxia Guo [ID] *[a]

Thanks to the characteristic hollow cavity structure and sustainable and nontoxic macrocycle molecule feature, cyclodextrins have been used as building block to fabricate organic solvent nanofiltration (OSN) membranes with enhanced permeability and selectivity. Herein, hydroxypropyl-β-cyclodextrin (HP-β-CD) was incorporated into a poly(ether-*block*-amide) (Pebax) layer on a polysulfone support, followed by crosslinking with toluene 2,4-diisocyanate to prepare a crosslinked HP-β-CD/Pebax (CHP) membrane. By adjusting the initial HP-β-CD concentration (x) and crosslinking reaction time (y), the microporous structure and surface morphology of CHP_{x-y} ($x = 0, 0.25, 0.5, 0.75$; $y = 5, 10, 15$) membranes could be manipulated. The OSN performances of the CHP_{x-y} membranes were evaluated by the removal of dyes in methanol solution. The results revealed that the optimal $\text{CHP}_{0.5-10}$ membrane exhibited a high methanol permeance of 8.7 L m^{-2} h^{-1} bar^{-1}, high dye rejection (>96%), and high running stability (at least 336 h), due to the intrinsically microporous structure and surface morphology. This work would inspire the further development of cyclodextrins and other macrocyclic molecules in the preparation of OSN membranes and provide a promising strategy to fabricate state-of-the-art membranes for the efficient separation of organic solvent reclamation and removal of organic pollutants.

1 Introduction

The chemical and pharmaceutical industries usually face issues with the utilization and recovery or disposal of numerous organic solvents.[1–4] With increasingly stringent environmental laws, the reasonable separation, recovery, and treatment of organic solvents used have become a key focus of attention. In conventional chemical engineering processes, the separation and purification of chemical mixtures are often performed by extraction and distillation technologies based on the chemical properties of the materials,[5] which are often high-energy-consumption, high time-cost, and expensive approaches. Hence, it is very necessary to develop efficient and cheaper ways regardless of heat and phase transition to separate chemical mixtures. Based on these facts and industrial requirements, economical and sustainable membrane-based separation technologies are being widely explored and applied in the chemical, petrochemical, pharmaceutical, textile, printing, and dyeing industries.

Organic solvent nanofiltration (OSN), a pressure-driven membrane process to separate liquid organic solvents from the mixture at the end of the process,[6,7] is a promising technology that represents an energy-saving and high-efficiency separation process. Many polymers with higher chemical resistance have been used to fabricate OSN membranes for their applications. For instance, polysulfone (PS) was used as an aromatic polymer network to prepare a solvent-resistant nanofiltration membrane *via* the phase-inversion process employing immersion precipitation for the separation of isopropanol and rose Bengal.[8] The OSN membranes composed of poly(ether-ether-ketone) with/without surface modification exhibited excellent resistance towards polar aprotic solvents, acids, and bases,[9] as well as rose Bengal in isopropanol and acetone.[10] Polyimide-based OSN membranes with or without polyethylene glycol (PEG) modification or inorganic fillers performed exceptionally well in the polar aprotic solvents, such as dichloromethane (DCM), isopropanol (IPA), tetrahydrofuran (THF), *n*-methyl pyrrolidone (NMP), dimethylformamide (DMF), and dimethyl sulfoxide (DMSO).[11–14] In addition, polyamide-based thin film polyethylene OSN membranes,[15] zeolite-filled polydimethylsiloxane (PDMS),[16] fluoropolymers (*e.g.* PVDF),[17] polyacrylonitrile (PAN),[18–20] polybenzimidazole,[21–25] and poly(ether-*block*-amide) (Pebax) OSN membranes with or without surface decoration[26–28] have also been widely developed and showed high OSN performances. These results indicate that high OSN

[a]Faculty of Materials and Manufacturing, Beijing University of Technology, Beijing 100124, P. R. China. E-mail: hxguo@bjut.edu.cn

[b]Institut für Anorganische Chemie, Eberhard Karls Universität Tübingen, Auf der Morgenstelle 18, 72076 Tübingen, Germany. E-mail: yucang.liang@uni-tuebingen.de

performances depend upon not only the intrinsic chemical stability of the membrane polymer itself but also the solvent stability relevant to the chemical structure of the polymer and the presence of certain structural elements, like aromatic groups, ether bonds, or imide bonds.[29] Among these polymers, Pebax is a promising membrane material due to the combination of rigid polyamide (PA) segments as the ''bone'' and flexible polyether (PE) segments as the ''muscle'' giving it high mechanical strength, swelling resistance, thermal stability, and high permeability[30,31] as well as a good solvent affinity.[26] Lots of membranes based on Pebax polymer have been reported and utilized in pervaporation,[31–35] gas,[36–43] and other membrane-based pressure-driven separation processes.[26–28] In our previous work, Pebax was coated on a PS ultrafiltration substrate to form a PS/Pebax thin film composite (TFC) membrane, which showed high rejection and good permeance in the OSN separation of Evans blue from methanol solution.[27] The thin film composite membrane was prepared *via* the deposition of Pebax on a PAN support and then crosslinked by toluene diisocyanate (TDI) for the retention of brilliant blue from ethanol or DMF solution. However, despite the incorporation of graphene oxide (GO) nanosheets into the Pebax coating to enhance the membrane permeance,[26] the optimal GO-loaded Pebax membrane exhibited an ethanol permeance of just 1.9 L m^{-2} h^{-1} bar^{-1}.

Cyclodextrins (CDs), as cyclic oligomers of glucose, are composed of a hydrophilic external surface and hydrophobic cavity. The hydrophobic cavity of CDs is often used as a pathway for nonpolar organic solvents and the adjustment of the cavity size can effectively enhance the permeation ability. Moreover, the external surface of CDs can be functionalized by diverse pendant groups or by reaction of the external hydroxyl group with other molecules. It was reported that nanofilms prepared by the reaction of CDs and trimesoyl chloride (TMC) exhibited exceptionally high permeance for both polar and nonpolar solvents.[44] CDs were embedded into hydrophilic polyethyleneimine (PEI) to form a thin film nanocomposite membrane, showing enhanced OSN performance.[45] In addition, the interfacial polymerization of β-CD with a hydrocarbon-based terephtaloyl chloride (TC) on top of PAN porous supports formed a β-CD membrane, which showed fast solvent transport and shape-selective permeability in OSN applications and salt/dyes nanofiltration.[46,47] Nonetheless, due to the large molecular structure, easy agglomeration, low activity of hydroxyl groups, and low solubility of β-CD in neutral aqueous solution, its dissolution is required under a strong alkaline environment.[47] Considering these drawbacks of β-CD as a membrane material, the derivatives of hydroxypropyl β-CD (HP-β-CD) with hydroxyl groups in the side chain could achieve various mass ratios in an aqueous solution. Hence, HP-β-CD was incorporated into a polyamide skin layer by the interfacial polymerization of piperazine and trimesoyl chloride, endowing the resultant composite NF membrane nanocavity with enhanced permeability and divalent to monovalent ion selectivity.[48] However, the separation performance of the OSN membranes incorporated with nanocavities of HP-β-CD is still unknown.

Consequently, in this work, HP-β-CD was incorporated into the Pebax layers on PS substrate and then crosslinked by TDI to form a nanocavity-contained HP-β-CD/Pebax (CHP) OSN membrane (Scheme 1). By adjusting the initial concentration (x) of HP-β-CD and the crosslinking reaction time (y), the composite, intrinsically microporous structure and surface morphology of CHP$_{x-y}$ ($x = 0, 0.25, 0.5, 0.75$; $y = 5, 10, 15$) membranes could be manipulated. By measuring the OSN performance of CHP$_{x-y}$ membranes for Evans blue and other dyes in methanol solution, CHP$_{0.5-10}$ membrane was found to be the optimal membrane and displayed a high methanol permeance of 8.7 L per (m^2 h bar), high dye rejection (>96%), and high stability (336 h continuous running), due to its intrinsically microporous structure and surface morphology. This work has inspired our further exploration of cyclodextrins and other
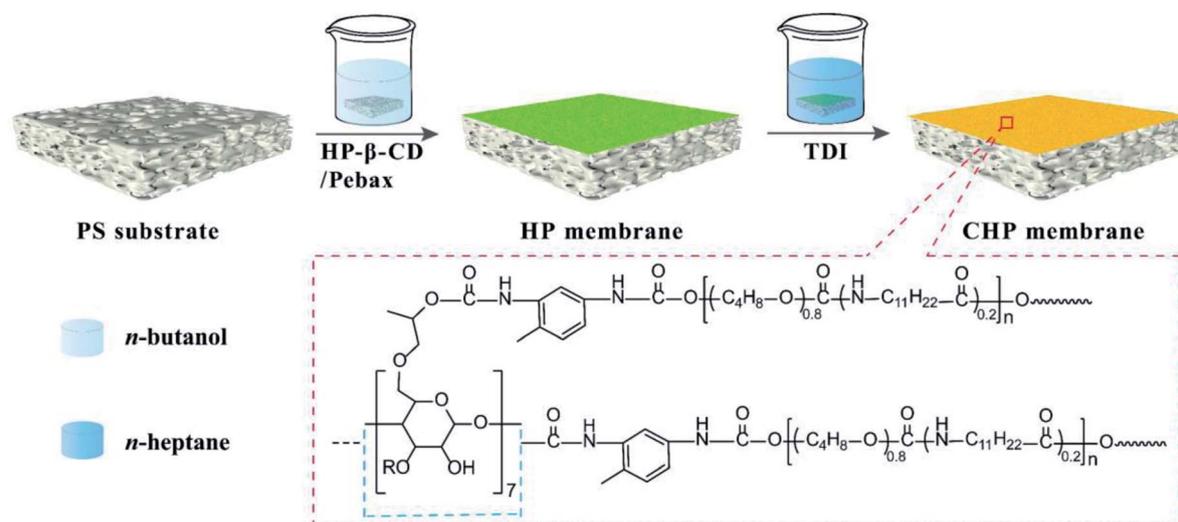
Scheme 1 Schematic of the preparation of the crosslinked CHP membrane.

macrocyclic molecules in the preparation of OSN membranes. The present work also provides a promising strategy to fabricate state-of-the-art membranes for the efficient separation of organic solvent for reclamation and for the removal of organic pollutants.

2 Experimental section

2.1 Materials and reagents

HP-β-CD was purchased from Shandong Binzhou Zhiyuan Biotechnology Co. Ltd. (Shandong, China). Pebax 2533 was commercially supplied by Arkema Inc. (France). TDI and n-heptane were obtained from Fuchen Chemical Reagent Co. Ltd. (Tianjin, China). Evans blue (EB), methyl blue (MB), Congo red (CR), acid fuchsin (AF), Eriochrome black T (EBT), and rhodamine B (RB) were purchased from Sigma-Aldrich (USA). Absolute ethanol, methanol, n-butanol, cyclohexane, and n-hexane were provided by Tianjin Kermel Chemistry Co., Ltd. (Tianjin, China). The commercial PS ultrafiltration membrane with a molecular weight cut-off (MWCO) of 2×10^5 kDa was provided by Beijing Separate Equipment Co. Ltd. (Beijing, China) and used as a substrate membrane to fabricate the OSN membranes. Before being used, the PS substrate membrane was soaked in anhydrous ethanol for 24 h and dried naturally at room temperature. Deionized (DI) water (18.25 MΩ cm) was used throughout all the experiments.

2.2 Fabrication of the crosslinked HP-β-CD/Pebax (CHP) OSN membranes

The fabrication process of the CHP OSN membrane is depicted in Scheme 1. Briefly, Pebax 2533 in n-butanol was stirred at 70 °C for 4 h to prepare 1.0 wt% Pebax 2533 n-butanol solution. HP-β-CD powder with 0.25, 0.5, and 0.75 wt% to the total mass was then added into the Pebax solution at 70 °C under stirring to form a homogeneous and transparent solution. Subsequently, a well-cleaned PS membrane substrate was immersed into the HP-β-CD and Pebax in n-butanol solution for 3 min. This was then taken out and dried at room temperature to obtain the HP-β-CD/Pebax (HP) membrane on PS substrate. For the crosslinking reaction, the HP membrane was immersed into a 1.0 wt% TDI of n-heptane solution at room temperature for 5–15 min. After being taken out and dried, the crosslinked HP-β-CD/Pebax (CHP) membrane was obtained. Depending on the concentration (x) of HP-β-CD and the crosslinking reaction time (y) used, the obtained membranes were denoted as CHP$_{x-y}$ (x = 0, 0.25, 0.5, 0.75, y = 5, 10, 15).

2.3 Characterizations

The surface chemical compositions of the as-prepared membranes were characterized by Fourier transform infrared (FTIR) spectroscopy (Vertex-70, Bruker, Germany) and X-ray photoelectron spectrometry (XPS, Thermo Escalab 250, USA). The surface and cross-sectional morphologies of the membranes were imaged by field-emission scanning electron microscopy (SEM, SU8020, Japan). The surface roughness of the membranes was analyzed by atomic force microscopy (AFM,

PicoScanTM2500, Agilent, USA) at 1×1 μm. The water contact angle (WCA) of the membranes was measured using a contact angle meter (DSA-100, Kruss, Germany).

2.4 OSN performance

The OSN performance was measured using self-made cross-flow filtration equipment with an effective membrane area of 22 cm^2. During the testing process, the membranes were pre-compacted at 4.0 bar for 3 h to reach a steady state, and then the OSN performance was tested at every 30 min interval. The permeance (P) and rejection rate (R) were calculated according to the following equations.

$$P = \frac{V}{AT\Delta P} \tag{1}$$

where V is the permeate volume (L), A is the effective area of the membrane (m^2), T is the filtration time, and ΔP is the operating pressure (bar).

$$R = \frac{C_f - C_p}{C_f} \times 100\% \tag{2}$$

where C_f and C_p are the concentrations of the feed and permeate solution, respectively. The concentration of the dye feed solution was 10 ppm, while the concentration of the permeate solution was detected by a UV-vis spectrophotometer (UV-3200, Mapada, Shanghai, China).

3 Results and discussion

3.1 Structure and morphologies of the membranes

The FTIR spectra of different membranes including the PS substrate, Pebax 2533 membrane, and CHP$_{x-10}$ (x = 0, 0.75) are shown in Fig. 1 and S1.† The FTIR spectrum of the PS substrate in Fig. 1a exhibited peaks at 1586 and 1488 cm^{-1}, which were assigned to the stretching vibration of C=C from the aromatic ring and the bending and scissoring of C–H bonds from –CH(CH$_3$)$_2$ groups, respectively.[48] The peak at 1325 cm^{-1} belonged to the characteristic vibration of a sulfone group from PS. The Pebax 2533 membrane on the PS substrate without TDI crosslinking (Fig. 1b) displayed a series of peaks at 1100 cm^{-1} (–C–O–C– stretching), 1538 cm^{-1} (bending of N–H in PA), 1640 cm^{-1} (stretching of –C=O in H–N–C=O), 1733 cm^{-1} (stretching of –C=O in PA), 2850 cm^{-1} and 2935 cm^{-1} (–C–H bending), and 3300 cm^{-1} (stretching of N–H in PA) (inset, Fig. 1).[26,27,49–51] Comparatively, after being crosslinked by TDI, the FTIR spectrum of the CHP$_{0-10}$ membrane without HP-β-CD (Fig. 1c) exhibited a shift in the tiny peak of Pebax at 1640 cm^{-1} in Fig. 1b to 1660 cm^{-1}, implying that the conjugation of the benzene ring of TDI would enhance the electron-donating ability of H–N–C=O groups, leading to the spectral blue-shift. The signal at 2269 cm^{-1} was assigned to the –N=C=O group of TDI.[26] After the incorporation of HP-β-CD into Pebax and following crosslinking with TDI, the spectrum of the CHP$_{0.75-10}$ membrane obtained (Fig. 1d) showed that the peak at 1100 cm^{-1} assigned to C–O–C group was intensified, due to introduction of more C–O–C groups from HP-β-CD.[44,45] Note that the intensity of the peak at 1660 cm^{-1} was slightly
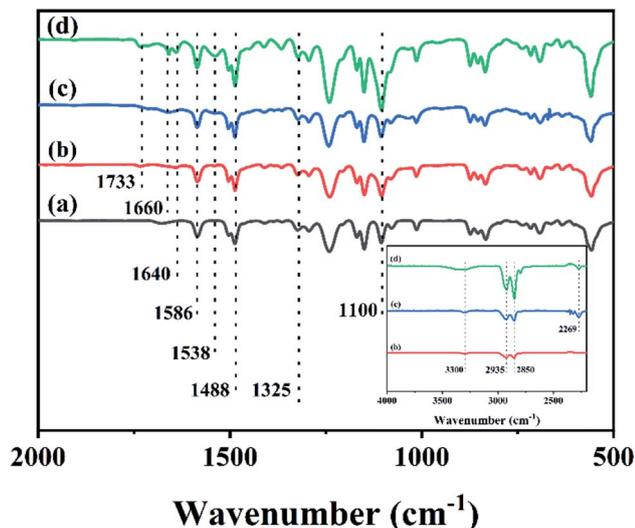
Fig. 1 FTIR spectra for the (a) PS substrate, (b) Pebax 2533 membrane, (c) CHP_{0-10} membrane and (d) $CHP_{0.75-10}$ membrane.

Table 1 XPS results of the CHP_{0-10} and $CHP_{0.5-10}$ membranes

Membrane	C (%)	O (%)	N (%)	O/N (%)
CHP_{0-10}	77.63	17.86	4.51	3.96
$CHP_{0.5-10}$	76.26	19.22	4.52	4.25

increased, but the peak at 2269 cm^{-1} attributed to –N=C=O bond of TDI was decreased, indicating the further crosslinking reaction between TDI and both Pebax as well as HP-β-CD. These results confirmed the formation of the crosslinked HP-β-CD/Pebax (CHP) layer on the PS substrate.

In addition, FTIR spectra on the reverse side of $CHP_{0.5-10}$ membrane were also measured. As shown in Fig. S2 (ESI),† it was clear that the IR spectrum of $CHP_{0.5-10}$ was consistent with the PS substrate. The characteristic absorption peaks of C–O–C at 1100 cm^{-1} from HP-β-CD and H–N–C=O at 1640 cm^{-1} from Pebax 2533 could not be found in the FTIR spectra of the reverse side of the $CHP_{0.5-10}$ membrane, clearly verifying that a selective layer mainly existed on the front side of the PS substrate.

To further explicate the elemental compositions of the CHP_{0-10} and $CHP_{0.5-10}$ membranes, XPS analysis was performed as shown in Fig. 2. As can be seen in Fig. 2a, both membranes presented three peaks at 531.92 (O 1s), 399.17 (N 1s), and 284.94 eV (C 1s). The elemental atomic percentages of carbon (C), oxygen (O), and nitrogen (N) on the membrane surface

listed in Table 1 show that the O/N ratio increased from 3.96% for the CHP_{0-10} membrane to 4.25% for the $CHP_{0.5-10}$ membrane. The increase in the O/N ratio of the HP-β-CD-incorporated membranes can be attributed to the high oxygen content of HP-β-CD (45.4 wt%). This indicated that HP-β-CD had been successfully incorporated into the Pebax selective layer. According to the high-resolution C 1s XPS spectra of the membranes (Fig. 2b, c and Table S1†), the proportion of O–C=O from polyurethane was remarkably increased from 3.37% to 5.54%. Also, the high-resolution N 1s and O 1s XPS spectra were further analyzed. As can be seen in Fig. S3a and b,† the N 1s peak from the high-resolution XPS was deconvoluted into three peaks at 397.5, 399.4, and 399.8 eV, which were attributed to the corresponding –N=C=O and C_{alkyl}–NH–C=O and C_{benzyl}–NH–C=O groups, respectively.[52] It is obvious that the N atom was bonded to three different C centres from the benzene ring, carbonyl, and saturated alkyl groups, respectively, showing slightly different binding energies. The proportion of C_{benzyl}–NH–C=O from polyurethane increased from 53.99% in the CHP_{0-10} membrane to 72.14% in the $CHP_{0.5-10}$ membrane. Similarly, the high-resolution O 1s XPS spectra (Fig. S3c and d†) clearly showed two peaks at 533.0 and 534.7 eV, which were attributed to the binding energy of C=O and C–O, respectively. Due to the addition of HP-β-CD, the proportion of C=O bonds formed by the crosslinking reaction of TDI with hydroxyl groups on the membrane surface increased from 6.12% for the CHP_{0-10} membranes to 10.74% for the $CHP_{0.5-10}$ membranes. All these results show that more TDI molecules participated in the crosslinking reaction to form the polyurethane structure with the incorporation of HP-β-CD, further verifying the successful crosslinking of TDI with HP-β-CD and Pebax.

The surface morphologies of the CHP_{x-10} ($x = 0, 0.25, 0.5, 0.75$) OSN membranes are shown in Fig. 3a. It was noted that
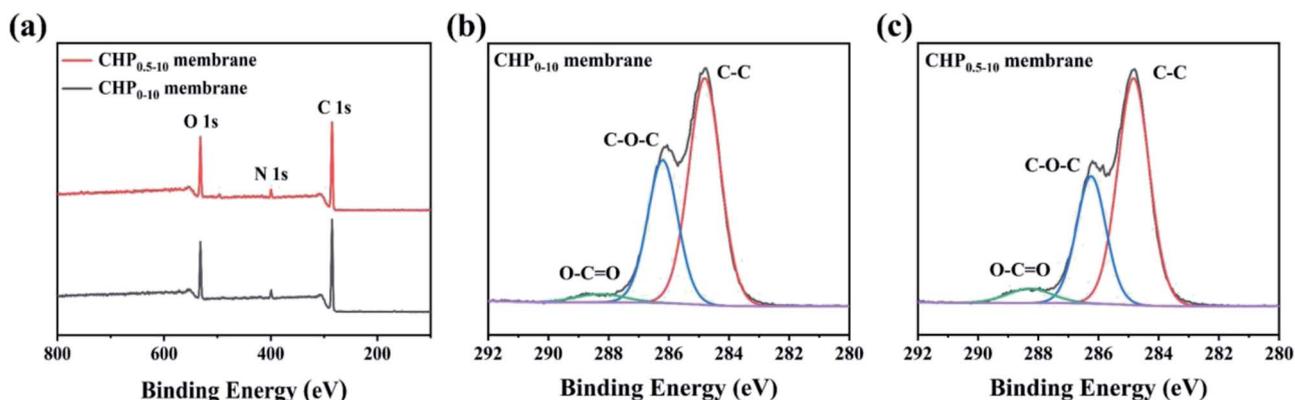

Fig. 2 (a) XPS survey spectra, (b and c) high-resolution C 1s spectra of the CHP_{0-10} and $CHP_{0.5-10}$ membranes, respectively.

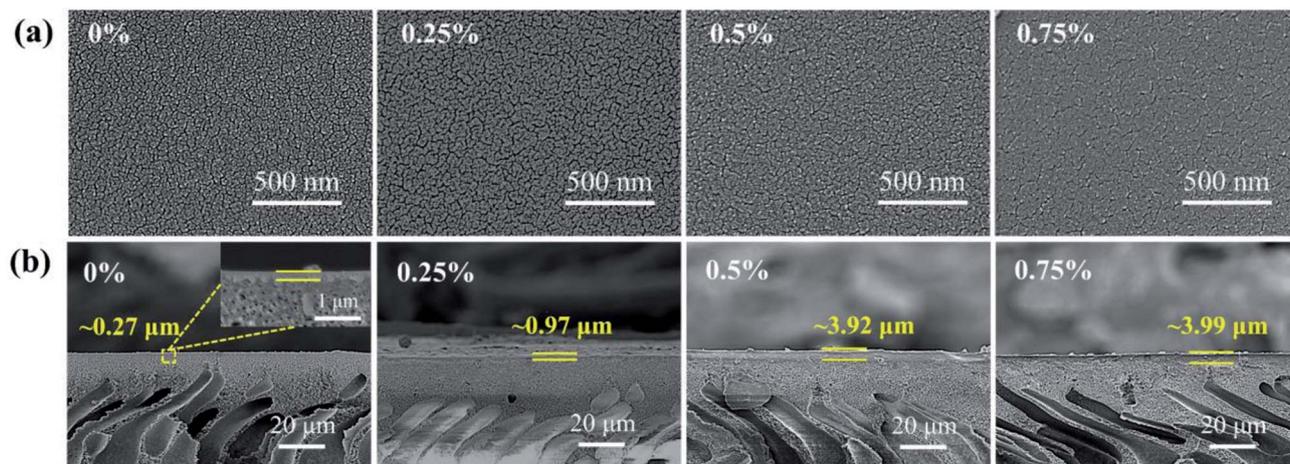© 2022 The Author(s). Published by the Royal Society of Chemistry

Fig. 3 (a) Surface and (b) cross-sectional SEM images of the CHP_{0-10}, $CHP_{0.25-10}$, $CHP_{0.5-10}$, and $CHP_{0.75-10}$ membranes.

the CHP_{0-10} membrane displayed a uniform textured surface, due to the nanoscale arrangement between the "soft" phase (polyether) and the glassy phase (polyamide) of Pebax caused by the crosslinking.[53] After the incorporation of 0.25 wt% HP-β-CD, the textural morphology of the $CHP_{0.25-10}$ membrane surface became more obvious. The texture image then became more compact with further increasing the HP-β-CD content to 0.50 and 0.75 wt% (Fig. 3a). The corresponding cross-sectional SEM images (Fig. 3b) indicated that the thickness of the CHP_{0-10} membrane without HP-β-CD was ~0.27 μm; however, with increasing the HP-β-CD content from 0.25 to 0.75 wt%, the thickness of the CHP_{x-10} ($x = 0.25, 0.5, 0.75$) membranes was gradually elevated to ~0.97, ~3.92, and ~3.99 μm, respectively. This result was mainly attributed to the host–guest interaction of HP-β-CD with the polyether chains and hydrogen bond interaction with Pebax.[54] This would lead to an increased microphase separation, leading to a more obvious texture morphology (Fig. 3a).[55] In addition, the crosslinking reaction would occur not only between TDI and Pebax but also between TDI and HP-β-CD, which was verified by the FTIR spectra in Fig. 1 and XPS results in Fig. 2. With increasing the HP-β-CD content, strong hydrogen bond interactions and crosslinking reactions induced the formation of a more compact layer of membranes (Fig. 3a). Hence, the thickness of the membranes

CHP_{x-10} ($x = 0.25, 0.5, 0.75$) increased with the corresponding increase in the HP-β-CD concentration in the casting solution.

The three-dimensional (3D) topology of the CHP_{x-10} ($x = 0, 0.25, 0.5, 0.75$) membrane surface was further probed by AFM to detect the surface roughness (R_a). As shown in Fig. 4, the surface roughness displayed an initial increase and then decreased with the variation in the HP-β-CD amount. With increasing HP-β-CD from 0 to 0.50 wt%, the R_a value of the CHP_{x-10} ($x = 0, 0.25, 0.5$) membranes increased from 3.2 to 3.7 nm due to the promoted microphase separation between the Pebax segments and HP-β-CD crosslinked by TDI. When the HP-β-CD content was increased to 0.75%, the R_a value of the $CHP_{0.75-10}$ membrane dropped sharply to 2.7 nm. This was probably due to HP-β-CD being relatively compatible with polyether chains and having a strong interaction with Pebax via hydrogen bonds, which drove the local regular arrangement of polymer chains,[54] leading to the formation of a more smooth surface with reduced roughness.

The surface wettability and electrical charges of the fabricated membranes were respectively characterized by their water contact angles (WCA) and zeta potential. As shown in Fig. 5, the WCA of the CHP_{0-10} membrane was around 88.0° due to the fewer hydroxyl groups on the membrane surface through the crosslinking. However, with increasing the HP-β-CD amount,
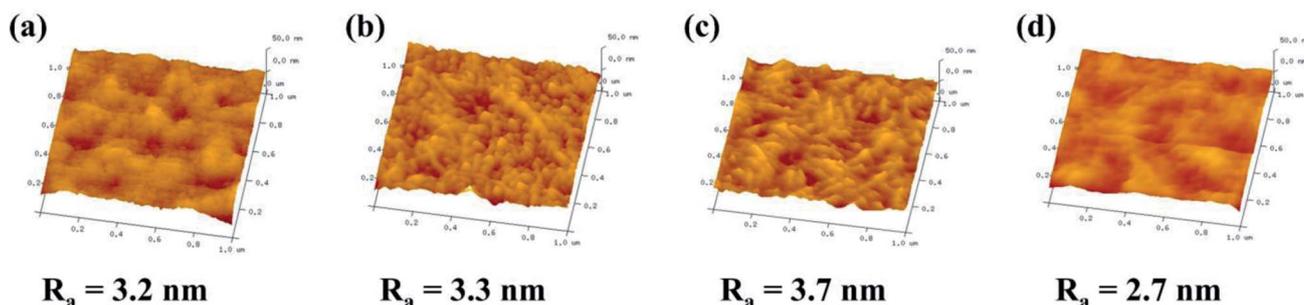

Fig. 4 AFM images of the: (a) CHP_{0-10}, (b) $CHP_{0.25-10}$, (c) $CHP_{0.5-10}$, and (d) $CHP_{0.75-10}$ membranes.
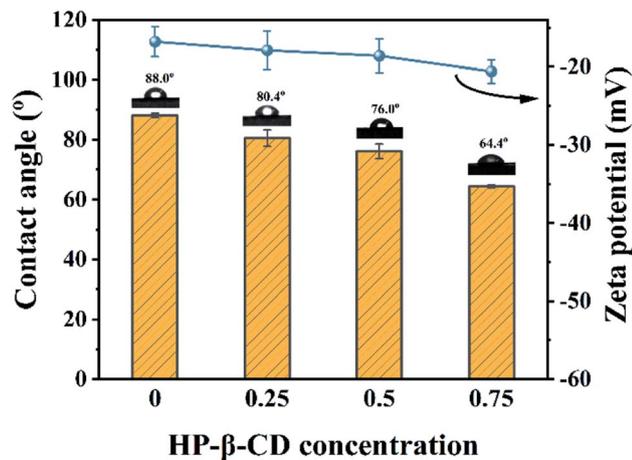
Fig. 5 Surface wettability and zeta potential of the CHP$_{x-10}$ membranes (x = 0, 0.25, 0.5, 0.75).

the WCA decreased from 80.4° for the CHP$_{0.25-10}$ membrane to 76.0° for the CHP$_{0.5-10}$ membrane, and to 64.4° for the CHP$_{0.75-10}$ membrane, indicating the significant improvement of the hydrophilicity of the CHP$_{x-10}$ membrane, due to the existence of a great number of hydroxyl groups from HP-β-CD in the membrane. Moreover, with increasing the HP-β-CD content, the zeta potential of the membranes in Fig. 5 also gradually decreased from −16.8 mV for the CHP$_{0-10}$ membrane to −18.6 mV for the CHP$_{0.5-10}$ membrane and −20.6 mV for the CHP$_{0.75-10}$ membrane, due to the introduction of more HP-β-CD, which would introduce more hydroxy groups into the membrane, leading to a more hydrophilic and more negative surface. Note that even when the crosslinking degree increased (TDI simultaneously reacted with hydroxyl groups from HP-β-CD and Pebax 2533), all the hydroxyl groups from HP-β-CD could not be completely consumed, and a great number of hydroxyl groups were still preserved in the membrane surface. As a result, the improvements in the hydrophilicity and surface electronegativity of the CHP$_{0.75-10}$ membrane directly led to a remarkably declined WCA and a low negative zeta potential.

3.2 Optimization of the CHP membranes

The HP-β-CD concentration (x) and crosslinking time (y) of TDI were investigated to optimize the OSN performances of the CHP membranes. When the crosslinking reaction time was 10 min, the separation properties of the CHP$_{x-10}$ membranes prepared with different HP-β-CD concentrations were tested using 10 ppm EB methanol solution at 20 °C under 4.0 bar. As shown in Fig. 6a, the methanol permeance of the CHP$_{0-10}$ membrane was 5.1 L per (m^2 h bar), with a rejection of 93%. When the mass ratio of HP-β-CD was 0.5 wt%, the CHP$_{0.5-10}$ membrane exhibited a 96% rejection rate accompanied with the highest methanol permeance of 8.9 L per (m^2 h bar). These results indicated that the incorporation of HP-β-CD into Pebax was conducive to the enhancement of the membrane rejection and methanol permeance. However, when further increasing the HP-β-CD mass ratio to 0.75 wt%, the methanol permeance of the CHP$_{0.75-10}$ membrane decreased and the corresponding rejection rate increased. The reason for this was probably due to the more compact selective layer (Fig. 3a) and less rough membrane surface (Fig. 4d), leading to a decreased methanol permeability. The enhanced rejection of the CHP$_{x-10}$ membranes could be assigned to the increased surface negatively charge (Fig. 5), which correspondingly increased the electrostatic repulsion between the solute and the membrane surface. In other words, the Donnan exclusion effects between the surface and the charged molecule played an important role. The high permeability of the as-prepared CHP$_{x-10}$ membranes could be ascribed to the surface properties of the top selective layer and the inner cavity size of the membrane formed by the appropriate incorporation of HP-β-CD. First, the improvement of the surface hydrophilicity with increasing the HP-β-CD content, as shown in Fig. 5, was beneficial for polar solvent transport through the membrane.[56] Second, the inner cavity size of HP-β-CD as a nanochannel on the membrane directly influenced the transport of methanol in the active layer.[44] Third, increasing the surface roughness further increased the methanol permeance; thus, an increase in the methanol permeance was achieved. Though the increase in the thickness of the active layer, as shown in Fig. 4b, will increase the transport resistance,
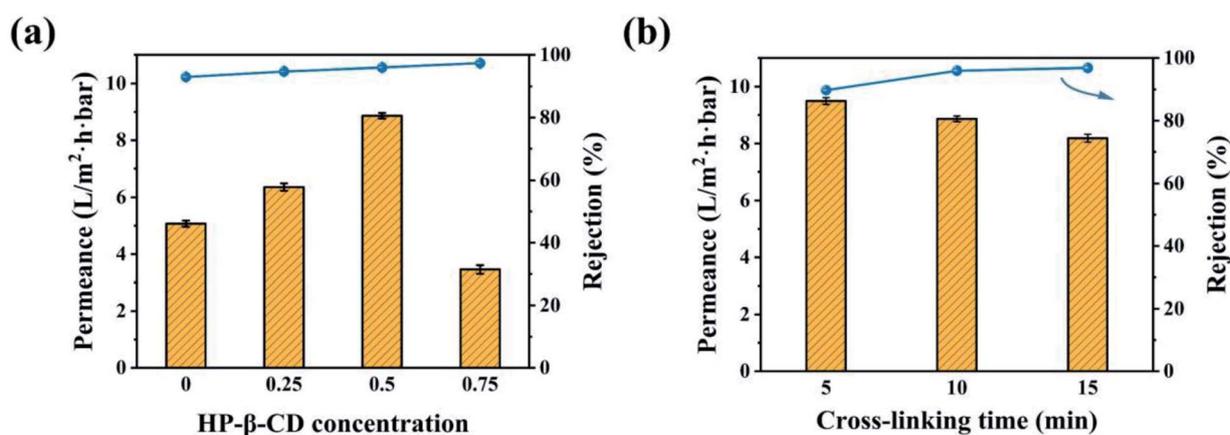

Fig. 6 OSN performances of the: (a) CHP$_{x-10}$ membranes (x = 0, 0.25, 0.5, 0.75) and (b) CHP$_{0.5-y}$ membranes (y = 5, 10, 15) for EB in methanol solution.

the limited increment was insufficient to hinder the permeance improvement. Therefore, the permeance of the CHP$_{x–10}$ membranes showed an improvement under the combined effects of roughness, hydrophilicity, and the HP-β-CD content.

When the mass ratio of HP-β-CD was fixed at 0.5 wt%, a series of CHP$_{0.5–y}$ membranes were prepared by controlling the cross-linking reaction times from 5 min to 15 min. The OSN performances of the resulting CHP$_{0.5–y}$ membranes were investigated as shown in Fig. 6b. It was found that a longer reaction time led to a high rejection rate with a low permeance, possibly due to a high crosslinking degree on the membrane.[52] XPS spectroscopy was used to demonstrate the variation of the crosslinking degree of the CHP$_{0.5–5}$ and CHP$_{0.5–15}$ membranes.[52] As shown in Fig. S4,† the high-resolution C 1s XPS spectra clearly showed that the proportion (5.97%) of O–C=O species in the CHP$_{0.5–15}$ membrane was higher than 3.40% in the CHP$_{0.5–5}$ membrane, indicating a gradual increase in the degree of crosslinking with increasing the crosslinking time. Therefore, when the cross-linking time increased from 5 to 15 min, the methanol permeance of the membrane markedly decreased from 9.5 to 8.2 L per (m^2 h bar), while the rejection rate increased from 89.76% to 96.87%. Based on the above-mentioned results, HP-β-CD concentration of 0.5 wt% and the crosslinking time of 10 min were optimal conditions for the preparation of the CHP$_{0.5–10}$ membrane.

3.3 Separation performance of the CHP$_{0.5–10}$ membrane

The OSN permeances of polar and nonpolar solvents, including methanol (MeOH), ethanol (EtOH), isopropanol (IPA), cyclohexane, and *n*-hexane, were further investigated using the CHP$_{0.5–10}$ membrane at ambient conditions. As can be seen from Fig. 7a, the membrane exhibited considerable high permeance for nonpolar solvents, such as a cyclohexane permeance of 6.8 L per (m^2 h bar) and *n*-hexane permeance of 13.6 L per (m^2 h bar), meanwhile, for polar solvents, the permeance in order was: MeOH (9.2 L per (m^2 h bar)) > EtOH (6.7 L per (m^2 h bar)) > IPA (3.8 L per (m^2 h bar)). The difference in permeance might be related to the solvent's intrinsic properties, such as viscosity,

kinetic diameter, and solubility parameter, as shown in Table S2.† Generally, solvent molecules with a lower viscosity, smaller molar diameter, and solubility parameters similar to the separation layer can more easily penetrate through membranes. Also, the permeance of the hydrophobic membrane increased as the polarity of the solvent decreased, while the permeance of the hydrophilic membrane decreased as the polarity of the solvent decreased.[56] Although the as-prepared CHP membranes were hydrophilic (Fig. 5), the high permeance for cyclohexane and *n*-hexane was mainly due to the hydrophobic inner cavity of HP-β-CD having an excellent affinity towards cyclohexane and *n*-hexane.[44] However, the permeance of *n*-hexane was higher than that of cyclohexane, which was primarily attributed to the viscosity of *n*-hexane (0.29 (10^{-3} Pa s)) being much lower than that of cyclohexane (0.94 (10^{-3} Pa s)). For polar solvents, the kinetic diameters, following the trend of MeOH (0.51 nm) < EtOH (0.57 nm) < IPA (0.62 nm), was exactly the opposite order from their permeance. This may be due to the hydroxyl (–OH) groups on the exterior of HP-β-CD cavities forming a relatively hydrophilic space between HP-β-CD and Pebax with a high affinity towards polar organic solvents. Another important reason is that the cavity size of β-CD (0.60 nm) could allow MeOH (0.51 nm) and EtOH (0.57 nm) to migrate across but not IPA (0.62 nm),[45] resulting in a high permeance for MeOH and EtOH.

Furthermore, the separation performance of the CHP$_{0.5–10}$ membrane was further investigated by MeOH solutions of different dyes, including Eriochrome black T (EBT), rhodamine B (RB), acid fuchsin (AF), Congo red (CR), methyl blue (MB), and Evans blue (EB). Table S3 (ESI)† illustrates the chemical structures and molecular weights of these dyes. As shown in Fig. 7b, the rejection order of the negatively charged dyes was EB (96.0%, M_w = 961 Da) > MB (92.9%, M_w = 800 Da) > CR (89.5%, M_w = 697 Da) > AF (79.7%, M_w = 585 Da) > EBT (36.3%, M_w = 461 Da). This indicated that the rejection of the CHP$_{0.5–10}$ membrane generally increased with the increasing molecular weight of dyes. However, the rejection of RB (around 2.0%) was lower than that of EBT, although the molecular weight of RB (M_w = 479 Da) was larger
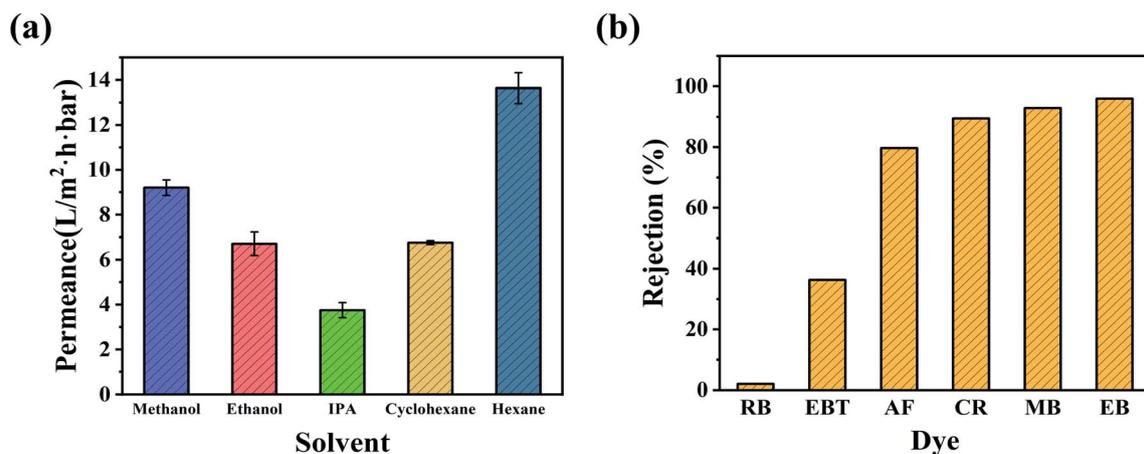

Fig. 7 (a) Nanofiltration performance of polar and nonpolar solvents for the CHP$_{0.5–10}$ membrane. (b) Rejection of dyes with different molecular weights through the CHP$_{0.5–10}$ membrane.
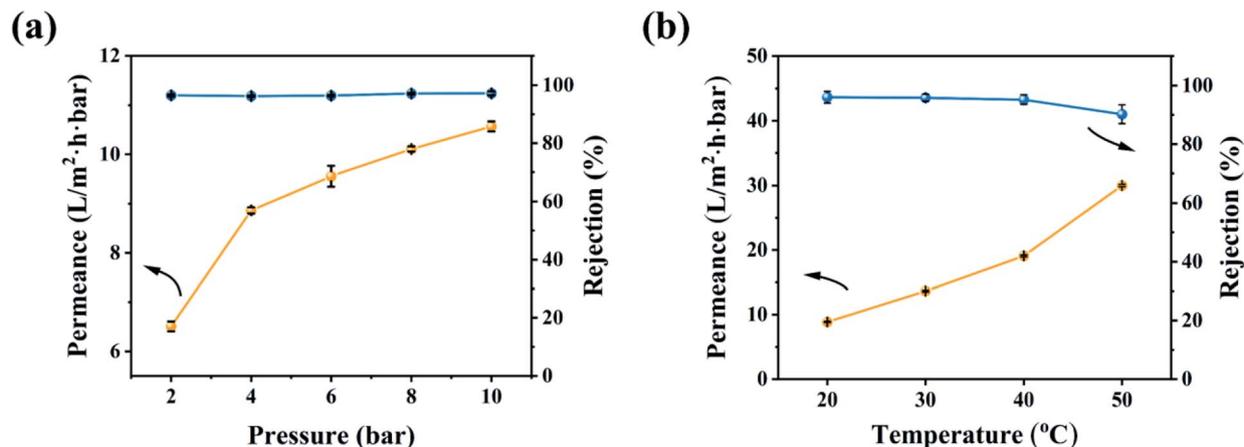
Fig. 8 OSN performance of the CHP$_{0.5-10}$ membrane for EB in methanol solution under (a) various operating pressures and (b) different temperatures.

than that of EBT ($M_w = 461$ Da, 36.3%). The low rejection of RB might be related to the positive charge of RB in methanol,[57,58] which can more easily pass through the membrane. According to the electric charges of the dyes and zeta potential of the CHP membrane in Fig. 5, there was a Donnan effect between the negatively charged membrane and dye molecules. Thus, the rejection mechanism of the prepared membrane for dye molecules was mainly attributed to the molecular size effect and the Donnan effect. Fig. S5† further depicts the separation performance of the CHP$_{0.5-10}$ membrane for EB in EtOH (97.0%) and IPA (97.1%). These high rejection rates indicated that the CHP$_{0.5-10}$ membrane has excellent potential for organic solvent nanofiltration.

The effect of the operating conditions on the OSN performance was further investigated in Fig. 8. With increasing the operating pressure, the permeability of the CHP$_{0.5-10}$ membrane increased and EB rejection was slightly changed

(Fig. 8a), due to the increment of the operating pressure reinforcing the driving force of the membrane and thereby increasing the permeability.[59] In general, an increase in pressure will cause the pores of the OSN membrane to shrink,[7,59] so the basically unchanged rejection rate showed that the CHP$_{0.5-10}$ membrane had excellent stability in a range of 2.0–10.0 bar. In addition, the increasing operating temperature could also increase the permeability (Fig. 8b). This behaviour may be explained by an enhancement of the methanol mass transfer coefficient,[60] thanks to the decrease in the temperature-dependent viscosity of the methanol solution. Moreover, with increasing the operating temperature, a dilatation in the pore sizes occurred, which facilitated the transport of solutes through the membrane and reduced the concentrations in the membrane pores and on the membrane surfaces.[60,61]

Based on the above-mentioned investigations, a comparison of the OSN performances among the optimal CHP$_{0.5-10}$

Table 2 Comparison of the OSN performances among the crosslinked HP-β-CD/Pebax (CHP$_{0.5-10}$) membrane and some reported OSN membranes[a,62]

Membrane	Solvent	Solute	Solvent permeance (L per m^2 per h per bar)	Rejection (%)	Reference
CHP$_{0.5-10}$	**Methanol**	**EB**	**9.2**	**96.0**	**This work**
	Ethanol		**6.7**	**97.0**	
	Isopropanol		**3.8**	**97.1**	
PBI/polyester support	Ethanol	RBB	3.69	~100	25 and 62
Pebax 1657/GO/PAN	Ethanol	BB	1.9 ± 0.012	95	26 and 62
Pebax 2533/PS	Methanol	EB	7.2	91.6	27 and 62
β-CD-TMC/Matrimid	Ethanol	RBB	3.1	95.7	44 and 62
PEI/β-CD/PAN	Isopropanol	PEG 1000	2.2	>93	45 and 62
β-CD-TC/PAN	Methanol	MO	5.8	93	47 and 62
PIM-1/PAN	Ethanol	Tetrazolium blue chloride	4.3	~92	62 and 63
PDA/P84	Ethanol	MB	~0.8–0.9	~99	62 and 64
PDA/β-CD/P84	Ethanol	MB	14.9	97.6	62 and 65
Polyamide 6 hollow fibre	Methanol	VB-12	0.27	96.3	62 and 66
PDA/PAN	Methanol	1.58–5.4 nm Au nanoparticles	~1.3	97.5	62 and 67
TTSBI-TMC/cross-linked P84 co-polyimide/PP support	Methanol	Crystal violet	6.0	98.7	62 and 68

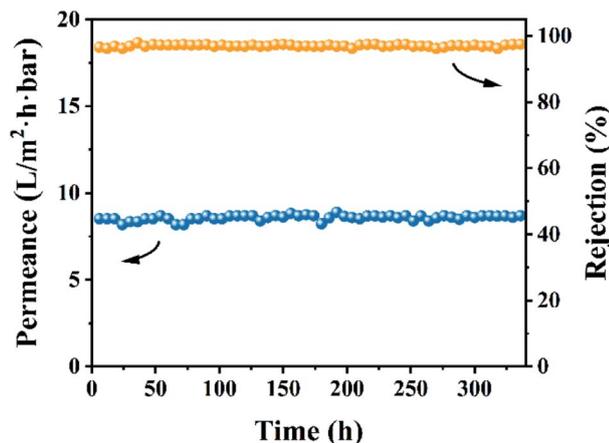[a] EB: Evans blue; BB: brilliant blue; RBB: Remazol brilliant blue; MO: methyl orange; MB: methyl blue.

Fig. 9 Stability performance of the $CHP_{0.5-10}$ membrane for EB in methanol solution.

membrane and the previously reported membranes[62] is presented in Table 2. The results indicated that the $CHP_{0.5-10}$ membranes were markedly superior to those in previous reports, revealing the outstanding effect of HP-β-CD in preparing an OSN membrane for potential application in the decolorization of textile dyeing industry effluent. Bruggen *et al.* reported previously that when the membrane was immersed in an organic solvent, the polymer chains might migrate on the membrane top layer, causing a change in the size and distribution of the membrane pores, thereby reducing the rejection rate.[56] Therefore, the long-term stability of the membrane was evaluated in 10 ppm EB methanol solution for consecutive running of 336 h. As shown in Fig. 9, the $CHP_{0.5-10}$ membrane still maintained a high rejection of about 96.0% and a high permeance of about 8.7 L per (m^2 h bar) during the test period, revealing the superior stability of the membrane for EB in methanol solution.

4 Conclusions

In summary, HP-β-CD was successfully incorporated into the Pebax layer on the PS support, and further polymerized with TDI to prepare a crosslinked HP-β-CD/Pebax (CHP) membrane. By adjusting the initial concentration (x) of HP-β-CD and the crosslinking reaction time (y), the composite, structure, and surface morphology of the CHP_{x-y} ($x = 0, 0.25, 0.5, 0.75; y = 5, 10, 15$) membranes obtained could be controlled, which was performed by the competitively interfacial crosslinking polymerizations of TDI with both HP-β-CD and Pebax 2533. Testing the OSN performance of the obtained CHP_{x-y} membranes confirmed that the $CHP_{0.5-10}$ membrane was an optimal membrane and indicated a high methanol permeance of 8.7 L per (m^2 h bar), high rejection for dyes (96.0% for EB, 92.9% for MB), and high stability (at least consecutive running for 336 h) in methanol solution, thanks to the intrinsic microporous structure fabricated by the incorporation of HP-β-CD into the 3D networks of the membrane. Especially, the $CHP_{0.5-10}$ membrane exhibited a higher rejection rate for the negatively

charged dye EBT with a molecular weight of 461 Da compared to that of the positively charged dye RB with a molecular weight of 479 Da, revealing the excellent rejection rate of the resulting $CHP_{0.5-10}$ membrane for the negatively charged solute. This work inspires the further development of cyclodextrins and other macrocyclic molecules for the preparation of OSN membranes and provides a promising strategy to fabricate state-of-the-art membranes for the efficient separation of solvents for reclamation, as well as organic pollutants removal and heavy metals, and drug purification.

Conflicts of interest

There are no conflicts to declare.

Acknowledgements

Notes and references

1 M. H. D. A. Farahani and T.-S. Chung, *Chem. Eng. J.*, 2018, **345**, 174–185.

2 C. Jiménez-González, A. D. Curzons, D. J. Constable and V. L. Cunningham, *Int. J. Life Cycle Assess.*, 2004, **9**, 114–121.

3 C. S. Slater, M. J. Savelski, W. A. Carole and D. J. Constable, *Green Chemistry in the Pharmaceutical Industry*, ed. P. J. Dunn, A. S. Wells and M. T. Williams, Wiley-VCH Verlag GmbH & Co. KGaA, Weinheim, Germany, 2010, ch. 3, pp. 49–82.

4 V. R. Veleva, B. W. Cue and S. Todorova, *ACS Sustainable Chem. Eng.*, 2017, **6**, 2–14.

5 D. S. Sholl and R. P. Lively, *Nature*, 2016, **532**, 435.

6 S. Hermans, H. Mariën, C. Van Goethem and I. F. J. Vankelecom, *Curr. Opin. Chem. Eng.*, 2015, **8**, 45–54.

7 P. Marchetti, M. F. Jimenez Solomon, G. Szekely and A. G. Livingston, *Chem. Rev.*, 2014, **114**, 10735–10806.

8 A. K. Hołda, B. Aernouts, W. Saeys and I. F. J. Vankelecom, *J. Membr. Sci.*, 2013, **442**, 196–205.

9 J. da Silva Burgal, L. G. Peeva, S. Kumbharkar and A. Livingston, *J. Membr. Sci.*, 2015, **479**, 105–116.

10 K. Hendrix, M. Van Eynde, G. Koeckelberghs and I. F. J. Vankelecom, *J. Membr. Sci.*, 2013, **447**, 212–221.

11 Z. F. Gao, G. M. Shi, Y. Cui and T.-S. Chung, *J. Membr. Sci.*, 2018, **565**, 169–178.

12 M. F. J. Solomon, Y. Bhole and A. G. Livingston, *J. Membr. Sci.*, 2012, **423–424**, 371–382.

13 Y. H. S. Toh, F. W. Lim and A. G. Livingston, *J. Membr. Sci.*, 2007, **301**, 3–10.

14 K. Vanherck, P. Vandezande, S. O. Aldea and I. F. J. Vankelecom, *J. Membr. Sci.*, 2008, **320**, 468–476.

15 S. H. Park, Y. J. Kim, S. J. Kwon, M. G. Shin, S. E. Nam, Y. H. Cho, Y. I. Park, J. F. Kim and J. H. Lee, *ACS Appl. Mater. Interfaces*, 2018, **10**, 44050–44058.

16 L. E. Gevers, I. F. Vankelecom and P. A. Jacobs, *Chem. Commun.*, 2005, 2500–2502.

17 A. Karimi, A. Khataee, M. Safarpour and V. Vatanpour, *Sep. Purif. Technol.*, 2020, **237**, 11635.

18 X. Li, S. De Feyter, D. Chen, S. Aldea, P. Vandezande, F. Du Prez and I. F. Vankelecom, *Chem. Mater.*, 2008, **20**, 3876–3883.

19 C. Linder, M. Perry, M. Nemas and R. Katraro, *US Pat.*, 5039421, 1991-8-13.

20 N. W. Oh, J. Jegal and K. H. Lee, *J. Appl. Polym. Sci.*, 2001, **80**, 1854–1862.

21 D. Chen, S. Yu, M. Yang, D. Li and X. Li, *RSC Adv.*, 2016, **6**, 16925–16932.

22 M. H. Davood, A. Farahani and T.-S. Chung, *Sep. Purif. Technol.*, 2019, **209**, 182–192.

23 G. Székely, I. B. Valtcheva, J. F. Kim and A. G. Livingston, *React. Funct. Polym.*, 2015, **86**, 215–224.

24 I. B. Valtcheva, P. Marchetti and A. G. Livingston, *J. Membr. Sci.*, 2015, **493**, 568–579.

25 D. Y. Xing, S. Y. Chan and T.-S. Chung, *Green Chem.*, 2014, **16**, 1383–1392.

26 J. Aburabie and K.-V. Peinemann, *J. Membr. Sci.*, 2017, **523**, 264–272.

27 Z. Liu, Z. Qin, S. Cui, M. Jia, Q. An, N. Wang, Y. Liu and H. Guo, *Chem. Ind. Eng. Prog.*, 2020, **39**, 2715–2723.

28 M. Sforca, S. Nunes and K.-V. Peinemann, *J. Membr. Sci.*, 1997, **135**, 179–186.

29 P. Vandezande, L. E. Gevers and I. F. Vankelecom, *Chem. Soc. Rev.*, 2008, **37**, 365–405.

30 R. Casadei, M. Giacinti Baschetti, M. J. Yoo, H. B. Park and L. Giorgini, *Membranes*, 2020, **10**, 188.

31 H. Yuan, X. Liu, S. Zhang and J. Lu, *Chem. Eng. Process.*, 2019, **144**, 107632–107639.

32 N. L. Le, Y. Wang and T.-S. Chung, *J. Membr. Sci.*, 2011, **379**, 174–183.

33 K. Liu, C.-J. Fang, Z.-Q. Li and M. Young, *J. Membr. Sci.*, 2014, **451**, 24–31.

34 A. E. Yildirim, N. D. Hilmioglu and S. Tulbentci, *Desalination*, 2008, **219**, 14–25.

35 Y. Zhang, Z. Jiang, J. Song, J. Song, F. Pan, P. Zhang and X. Cao, *Ind. Eng. Chem. Res.*, 2019, **58**, 16911–16921.

36 R. Casadei, M. Giacinti Baschetti, B. G. Rerolle, H. B. Park and L. Giorgini, *Polymer*, 2021, **228**, 123944.

37 M. Fakoori, A. Azdarpour, R. Abedini and B. Honarvar, *Korean J. Chem. Eng.*, 2021, **38**, 121–128.

38 J. Gao, H. Mao, H. Jin, C. Chen, A. Feldhoff and Y. Li, *Microporous Mesoporous Mater.*, 2020, **297**, 110030–110038.

39 E. G. Estahbanati, M. Omidkhah and A. E. Amooghin, *J. Ind. Eng. Chem.*, 2017, **51**, 77–89.

40 V. Nafisi and M. B. Hagg, *ACS Appl. Mater. Interfaces*, 2014, **6**, 15643–15652.

41 M. S. A. Wahab and A. R. Sunarti, *Int. J. Membr. Sci. Technol.*, 2015, **2**, 78–84.

42 P. D. Sutrisna, J. Hou, M. Y. Zulkifli, H. Li, Y. Zhang, W. Liang, D. M. D'Alessandro and V. Chen, *J. Mater. Chem. A*, 2018, **6**, 918–931.

43 W. Zhu, Y. Qin, Z. Wang, J. Zhang, R. Guo and X. Li, *J. Energy Chem.*, 2019, **31**, 1–10.

44 J. Liu, D. Hua, Y. Zhang, S. Japip and T. S. Chung, *Adv. Mater.*, 2018, **30**, 1705933–1705939.

45 H. Mao, H. Zhang, Y. Li, Y. Xue, F. Pei, J. Wang and J. Liu, *ACS Sustainable Chem. Eng.*, 2015, **3**, 1925–1933.

46 T. Huang, T. Puspasari, S. P. Nunes and K.-V. Peinemann, *Adv. Funct. Mater.*, 2019, **30**, 1906797–1906804.

47 L. F. Villalobos, T. Huang and K.-V. Peinemann, *Adv. Mater.*, 2017, **29**, 1606641–1606647.

48 Z. Yao, H. Guo, Z. Yang, W. Qing and C. Y. Tang, *Desalination*, 2018, **445**, 115–122.

49 L. M. Gradinaru, M. Barbalata-Mandru, M. Drobota, M. Aflori, M. Spiridon, G. Gradisteanu Pircalabioru, C. Bleotu, M. Butnaru and S. Vlad, *Nanomaterials*, 2020, **10**, 754–773.

50 J. Konieczny and K. Loos, *Polymers*, 2019, **11**, 256–265.

51 D. P. Nayak, A. M. Kotha, O. S. Yemul, S. Ponrathnam and R. C. Raman, *Biomacromolecules*, 2001, **2**, 1116–1123.

52 T. Huang, B. A. Moosa, P. Hoang, J. Liu, S. Chisca, G. Zhang, M. AlYami, N. M. Khashab and S. P. Nunes, *Nat. Commun.*, 2020, **11**, 5882.

53 A. Car, C. Stropnik, W. Yave and K.-V. Peinemann, *Adv. Funct. Mater.*, 2008, **18**, 2815–2823.

54 S. Uenuma, R. Maeda, H. Yokoyama and K. Ito, *Soft Matter*, 2020, **16**, 9035–9041.

55 Y. Zhang, Y. Shen, J. Hou, Y. Zhang, W. Fam, J. Liu, T. D. Bennett and V. Chen, *ACS Appl. Mater. Interfaces*, 2018, **10**, 20006–20013.

56 J. G. B. Van der Bruggen and C. Vandecasteele, *Chem. Eng. Sci.*, 2002, **57**, 2511–2518.

57 B. Li, Y. Cui, S. Japip, Z. Thong and T.-S. Chung, *Carbon*, 2018, **130**, 503–514.

58 Y. Lu, Z. Wang, W. Fang, Y. Zhu, Y. Zhang and J. Jin, *Ind. Eng. Chem. Res.*, 2020, **59**, 22533–22540.

59 W. Mickols, Z. Mai and B. van der Bruggen, *Desalination*, 2021, **501**, 114905–114918.

60 C. F. Couto, W. G. Moravia and M. C. S. Amaral, *Clean Technol. Environ. Policy*, 2017, **19**, 2057–2073.

61 S. R. Hosseinabadi, K. Wyns, V. Meynen, A. Buekenhoudt and B. Van der Bruggen, *J. Membr. Sci.*, 2016, **513**, 177–185.

62 G. M. Shi, Y. Feng, B. Li, H. M. Tham, J.-Y. Lai and T.-S. Chung, *Prog. Polym. Sci.*, 2021, **123**, 101470–101496.

63 J. Li, M. Zhang, W. Feng, L. Zhu and L. Zhang, *J. Membr. Sci.*, 2020, **601**, 117951–117958.

64 Y. Xu, F. You, H. Sun and L. Shao, *ACS Sustainable Chem. Eng.*, 2017, **5**, 5520–5528.

65 Y. Zhang, H. Sun, H. Sadam, Y. Liu and L. Shao, *Chem. Eng. J.*, 2019, **371**, 535–543.

66 S. Jeon, A. Nishitani, L. Cheng, L.-F. Fang, N. Kato, T. Shintani and H. Matsuyama, *RSC Adv.*, 2018, **8**, 19879–19882.

67 C. Zhang, Y. Lv, W. Z. Qiu, A. He and Z. K. Xu, *ACS Appl. Mater. Interfaces*, 2017, **9**, 14437–14444.

68 M. F. Jimenez-Solomon, Q. Song, K. E. Jelfs, M. Munoz-Ibanez and A. G. Livingston, *Nat. Mater.*, 2016, **15**, 760–767.